FLORE
Repository istituzionale dell'Università degli Studi di Firenze

Long-range paramagnetic NMR data can provide a closer look on metal coordination in metalloproteins

(Article begins on next page)

28 April 2024

Long-range paramagnetic NMR data can provide a closer look on metal coordination in metalloproteins*

Linda Cerofolini,[1] Tommaso Staderini,[2] Stefano Giuntini, [1,2] Enrico Ravera,[1,2] Marco Fragai,[1,2,3]
Giacomo Parigi,[1,2] Roberta Pierattelli,[1,2] Claudio Luchinat[1,2]*

1. Magnetic Resonance Center (CERM) and Interuniversity Consortium for Magnetic Resonance of Metallo Proteins (CIRMMP), Via L. Sacconi 6, 50019 Sesto Fiorentino, Italy,

2. Department of Chemistry "Ugo Schiff", University of Florence, Via della Lastruccia 3, 50019 Sesto Fiorentino, Italy,

3. Giotto Biotech S.R.L., Via Madonna del Piano 6, 50019 Sesto Fiorentino, Italy.

Corresponding author:

Claudio Luchinat

claudioluchinat@cerm.unifi.it

FAX +390554574923

*This work is dedicated to Helmut Sigel, a pioneer of bioinorganic chemistry and a lifelong friend, on the occasion of his 80th birthday.

Abstract

Paramagnetic NMR data can be profitably incorporated in structural refinement protocols of metalloproteins or metal-substituted proteins, mostly as distance or angle restraints. However, they could in principle provide much more information, because the magnetic susceptibility of a paramagnetic metal ion is largely determined by its coordination sphere. This information can in turn be used to evaluate changes occurring in the coordination sphere of the metal when ligands (e.g.: inhibitors) are bound to the protein. This gives an experimental handle on the molecular structure in the vicinity of the metal which falls in the so-called blind sphere.

The magnetic susceptibility anisotropy tensors of cobalt(II) and nickel(II) ions bound to human carbonic anhydrase II in free and inhibited forms have been determined. The change of the magnetic susceptibility anisotropy is directly linked to the binding mode of different ligands in the active site of the enzyme. Indication about the metal coordination sphere in the presence of an inhibitor in pharmaceutically-relevant proteins could be important in the design of selective drugs with a structure-based approach.

Introduction

The appeal of paramagnetism-based NMR data for the investigation of structure and dynamics in biological molecules is growing continuously. This is mostly due to the fact that paramagnetic restraints are long-range in nature and thus allow for the investigation of the complex architectures of biomolecules [1–10]. The presence of a paramagnetic metal ion in a protein introduces a contribution to the magnetic susceptibility of the protein that, in turn, influences the chemical shift of the protein nuclei in the NMR spectra. The paramagnetic contribution to the shift related to the magnetic susceptibility of a paramagnetic metal is called pseudo-contact shift (PCS). PCSs depend on the anisotropy of the paramagnetic susceptibility and on the nuclear coordinates of the NMR observed nuclei with respect to the metal position; therefore, they have been widely used as structural restraints, providing long-range, accurate and robust structural information. PCSs were first used to refine a protein structure in solution starting from an X-ray structure in 1995 [11], and to calculate *ab initio* the NMR structure of a paramagnetic protein, together with other NMR restraints, in 1996 [12]. Metalloproteins containing a diamagnetic metal can be made paramagnetic by substituting the native metal ion with a paramagnetic one, so that PCSs (possibly complemented by paramagnetic residual dipolar couplings, RDCs) can be available to refine the structure of the protein in solution [13, 14]. The attachment of paramagnetic tags to diamagnetic proteins extended the possibility to exploit the structural information content of PCSs and RDCs to biomolecular systems in general. Over the years, the use of these restraints was also implemented in the most used programs for the calculation of protein structures in solution [12, 15–18]. Recently, a novel approach has been proposed where PCSs and RDCs are provided as structural restraints together with the X-ray reflections to determine whether a single structure can account for both types of data, i.e. if a single structure can be a good model for the protein both in solution and in the solid state [19]. With respect to previous protocols, based on the search for the smallest perturbation of the crystallographic coordinates needed to account for the NMR data [14, 20, 21], this approach has the

advantage of using directly the primary data (i.e., the X-ray reflections rather than the derived nuclear coordinates) for the refinement.

The use of PCSs as structural restraints passes through the evaluation of the magnetic susceptibility anisotropy tensor ($\Delta\chi$) of the paramagnetic metal ion. This tensor can be easily calculated from PCS data if the structure of the molecule is available [22, 23]. Therefore, a structural model is usually employed to obtain a first estimate of the tensor, so that the latter is used together with the experimental PCSs to calculate a refined model, and so on, in an iterative fashion.

The structure refinement that is achieved with this approach concerns mainly the coordinates of protein nuclei for which PCSs are directly measured. This usually excludes the nuclei close to the paramagnetic metal ion, either because of the severe paramagnetic line broadening induced by many metals, which prevents their signal detectability, or because of the presence of contact contributions to the detected hyperfine shifts, so that PCSs are not available (but only the sum of PCSs and contact shifts) [24]. For this reason, the refinement achieved with PCSs usually does not include the ligand residues around the paramagnetic metal ion.

On the other hand, the anisotropy components of the magnetic susceptibility tensor and its axes directions depend on the electronic structure and on the coordination geometry of the paramagnetic metal ion. In fact, the orientation of the $\Delta\chi$ tensor axes is related to structural elements of the bonding geometry, in terms of number of ligand nuclei and coordination geometry of the metal center. In the presence of a non-degenerate ground state well separated from the excited states, the deviation of the g tensor from the free electron g_e, as well as the $\Delta\chi$ tensor, are predicted to be small, whereas in the presence of low-lying excited states, the spin-orbit coupling becomes very effective, so that the intrinsically anisotropic orbital contribution to the g values and to the magnetic susceptibility is expected to be large [24].

The relationship between $\Delta\chi$ tensor and coordination geometry has recently started to be more deeply investigated [25, 26], up to the point that the precision of the *ab initio* theoretical calculations

4

nowadays achievable can allow for reliable estimates of the $\Delta\chi$ tensors if an accurate structural model is available [27]. Therefore, we can envisage that a structure refinement at the metal site will become possible by looking for a matching between the $\Delta\chi$ tensor back-calculated from the experimental PCSs observed for nuclei far from the metal and the $\Delta\chi$ tensor theoretically predicted from the local structure at the metal site [28].

For monitoring the variation of the $\Delta\chi$ tensors as a result of changes in the metal coordination sphere we ideally need a protein that is able to coordinate different metal ions and for which a number of different ligands affecting the geometry of the metal site is available. We have thus selected human carbonic anhydrase II (hCAII) as model system. hCAII is a 260 residues metallo-enzyme, which catalyzes the fast interconversion of CO_2 and HCO_3^-. Furthermore, carbonic anhydrases are relevant pharmaceutical targets for a number of pathological conditions [29]. The active site of hCAII contains a tetracoordinated zinc(II) ion, that is bound to the nitrogen atoms of three histidine residues (His94, His96 and His119). The fourth ligand is either a water molecule or a hydroxide ion depending on pH. This ligand is involved in hydrogen bonding with Thr199 (Figure 1A). The native zinc ion can be easily substituted by other bipositive metal ions. For example, substitution with cobalt(II) preserves the enzymatic activity and has been widely used in the literature [30]. Other derivatives, such as those with copper(II), manganese(II), and nickel(II) ions, have been also largely investigated [31–38]. Carbonic anhydrases are interesting targets in a variety of pathologic conditions, therefore their interaction with several small molecules acting as inhibitors are known and characterized. Furthermore, hCAII is one of the first discovered anhydrases and several structures exist of its complex with different inhibitors. It is thus a good example for understanding how different poses of the ligands can affect the paramagnetic properties. In this case, the position of first-sphere ligand residues from the protein is not appreciably altered upon binding of the inhibitor molecules, which simplifies the analysis of the results. Proteins with a less rigid coordinating environment may undergo larger rearrangements around the metal center, and

this would be reflected in the differences in the magnetic susceptibility anisotropy tensor as well. In those cases the possibility of linking the electronic structure to the $\Delta\chi$ tensors would be a significant step forward.

The $\Delta\chi$ tensors of the high spin cobalt(II) and nickel(II) substituted hCAII as free enzyme and in the presence of different inhibitors (oxalate and/or furosemide, Figure 1B-C) are calculated from the experimentally collected $^1H^N$ PCSs. The data show that the size and orientation of the tensors largely depend on the type of metal ion and on the coordination geometry at the metal center. In particular, the increase in magnitude of the $\Delta\chi$ tensors of cobalt(II) and nickel(II) after binding of different protein inhibitors correlates with an increase of coordination number for cobalt(II) and a decrease for nickel(II).

Materials and methods

Protein preparation

The cobalt(II) and nickel(II) derivatives were obtained from the Zn(II) adduct by a demetallation/metallation approach. Zn(II)-hCAII was expressed and purified as previously reported [39–41], then the protein solution was dialyzed extensively against 10 mM HEPES, pH 7.2, 50 mM pyridine-2,6-dicarboxylic acid (PDA) buffer [41, 42]. After complete demetallation, the excess of PDA solution was removed by cyclic washings with 10 mM HEPES, pH 7.2 buffer using a 10000 MWCO Amicon Ultra-15 Centrifugal Filter Concentrator (MilliporeSigma). The paramagnetic proteins were prepared by monitoring the titration of the apo-enzyme with cobalt(II) and nickel(II) sulfate solutions, respectively, with 1D ^1H and 2D ^1H-^{15}N HSQC solution NMR spectra.

NMR measurements and analysis of pseudocontact shifts

All the experiments were acquired on a Bruker DRX NMR spectrometer operating at 500 MHz, ^{1}H Larmor frequency. All the spectra were processed with the Bruker TopSpin 2.0 software package and were analyzed with the program CARA (ETH Zürich).

The NMR experiments for the backbone assignment were performed at 310 K on a zinc(II)-hCAII buffered solution (50 mM TrisSO$_4$, pH 7.5) at the concentration of 0.4 mM. 2 D ^{1}H–^{15}N HSQC spectra were acquired for the different adducts [zinc(II), cobalt(II) and nickel(II)] of hCAII (~ 0.4 mM in 10 mM HEPES buffer solution) in the absence and in the presence of increasing concentration of ligands (oxalate or furosemide), for the evaluation of PCSs. During the addition of the oxalate ligand to the free protein [cobalt(II)-hCAII and zinc(II)-hCAII] a progressive shift of the signals was visible, as expected for a ligand in the fast exchange regime on the NMR timescale. The final concentration of oxalate added to the protein was 5 mM and 15 mM for cobalt(II)-hCAII and zinc(II)-hCAII, respectively. Instead, during the addition of furosemide to the protein solution [cobalt(II)-hCAII, nickel(II)-hCAII and zinc(II)-hCAII], the signals of the free protein disappeared progressively through the titration while the concentration of the ligand increased. At the same time, new cross-peaks corresponding to the protein–ligand adduct appeared in the spectra, and increased in intensity with increasing concentration of furosemide, up to the stoichiometric ratio, as expected for a high-affinity ligand in the slow-exchange regime on the NMR timescale.

The titrations of cobalt(II)-hCAII and zinc(II)-hCAII with oxalate were performed at pH 5.8, 303 K; the titrations of cobalt(II)-hCAII and zinc(II)-hCAII with furosemide were performed at pH 6.8, 298 K; instead the titrations of zinc(II)-hCAII and nickel(II)-hCAII with furosemide were performed at pH 8.0, 303 K. The experimental conditions were chosen to maximize the affinity of the selected ligands for the protein [30, 36].

The PCSs were calculated from the difference in the value of chemical shift between the paramagnetic [cobalt(II) or nickel(II)] and diamagnetic [zinc(II)] spectrum of the free proteins or at the maximum ligand concentration.

The assignment of the NMR signals of zinc(II)-hCAII was obtained by the analysis of standard triple resonance ^{1}H-detected NMR spectra (HNCA, CBCA(CO)NH, HNCACB, HNCO and HN(CA)CO). The assignment of zinc(II)-hCAII in the presence of the oxalate ligand was obtained following the progressive shift of the peaks during the titration. The assignment of the new peaks of zinc(II)-hCAII with furosemide was unambiguous for most of the residues; the agreement of the obtained chemical shift perturbation, between the free protein and the protein bound to furosemide, with the X-ray structure of zinc(II)-hCAII in the presence of furosemide (PDB: 1Z9Y) was then assessed [39]. Assignment of the signal of the paramagnetic spectra of the cobalt(II) and nickel(II) derivatives of hCAII, instead, was obtained following an iterative procedure. First the PCSs $\Delta\chi$ tensor was evaluated with the program FANTEN [22] from the best fit of a set of unambiguous PCSs. The prediction of new PCSs according to the tensor estimate assisted in the determination of new PCSs, and thus in the refinement of the tensor [23, 43]. Using this simple protocol, we were able to easily assign the 88% of the H^N of total non-proline residues for zinc(II)-hCAII, 68% and 72% for cobalt(II)-hCAII at pH 5.8 and 6.8, respectively, and 64% for nickel(II)-hCAII (see Tables S1-S4 in Supplementary material).

Results and discussion

A total of 165, 176, 160 and 174 PCSs were collected for the cobalt(II)-substituted hCAII at pH 5.8 and 6.8 and for its adducts with the oxalate and the furosemide ligands, respectively, and of 25 and 159 PCSs for the nickel(II)-substituted hCAII and for its adduct with furosemide, respectively (see Tables S5-S10 in Supplementary material). The free nickel(II) protein showed very small changes in the chemical shifts with respect to the zinc(II) form, and PCSs were considered reliable only if the shifts were similar in the

8

^{1}H and ^{15}N dimensions of the 2D ^{1}H-^{15}N HSQC spectrum. A different shift for the ^{1}H and the ^{15}N nuclei of the same residue may, indeed, be related to small structural changes between the two samples, which may be of the same order or larger than the PCSs themselves. The data were fitted against the highest resolution (0.9 Å) X-ray structure of zinc(II)-hCAII (PDB 3KS3) [44] to obtain the $\Delta\chi$ tensors with the program FANTEN [22]. The agreement in the correlation plots between experimental and calculated data was good in all cases (see Figure 2, where the Q values are reported) resulting in the best fit values for the axial and rhombic anisotropies components ($\Delta\chi_{ax}$ and $\Delta\chi_{rh}$) and tensor orientations (expressed as angles of the main axes directions with the metal-ligand directions) reported in Table 1. It is apparent that there is a sizable increase in the anisotropy of the magnetic susceptibility tensor upon binding of oxalate to cobalt(II)-hCAII, and upon binding of furosemide to nickel(II)-hCAII, whereas binding of furosemide to cobalt(II)-hCAII affects only marginally the size of the tensor.

Table 1. Tensor parameters calculated with the program FANTEN for the different hCAII adducts. The tensor orientations are expressed as angles of the principal axes directions with the metal-ligand direction, defined as the direction from the metal to the coordinating atom in the ligand.

	Co-hCAII pH 5.8	Co-hCAII-$C_2O_4^{2-}$ pH 5.8	Co-hCAII pH 6.8	Co-hCAII-furosemide pH 6.8	Ni-hCAII pH 8.0	Ni-hCAII-furosemide pH 8.0
$\Delta\chi_{ax}$ (10^{-32} m^3)	2.24 ± 0.02	6.54 ± 0.04(*)	2.81 ± 0.03	3.09 ± 0.02	0.25 ± 0.08 (*)	1.65 ± 0.03
$\Delta\chi_{rh}$ (10^{-32} m^3)	-1.18 ± 0.02	-4.44 ± 0.03(*)	-0.63 ± 0.02	-1.69 ± 0.02	-0.3 ± 0.1 (*)	-0.77 ± 0.02
x-His 96	$27 \pm 1°$	$70 \pm 0.5°$(*)	$32 \pm 1°$	$22 \pm 0.5°$	$54 \pm 19°$ (*)	$80 \pm 1°$
y-His 94	$26 \pm 1°$	$43 \pm 0.5°$(*)	$19 \pm 1°$	$7 \pm 0.5°$	$55 \pm 20°$ (*)	$80 \pm 1°$
z-His 119	$27 \pm 0.5°$	$80 \pm 0.2°$(*)	$33 \pm 0.2°$	$33 \pm 0.4°$	$77 \pm 13°$ (*)	$71 \pm 1°$

	Figure 3A	Figure 3B	Figure 3C	Figure 3D	Figure 3E	Figure 3F

(*) The standard convention of labeling the axes in order to have $|\Delta\chi_{rh}| \leq 2|\Delta\chi_{ax}|/3$ is not used here in order to better compare the directions where the magnetic susceptibility is larger (z-axis) or smaller (x-axis) (see [45] for a further discussion of this point).

NMR analysis of the cobalt(II)-substituted hCAII and its adducts with oxalate and furosemide.

The data show that the anisotropy of the tensor for the free cobalt(II)-hCAII slightly increases on passing from pH 5.8 to pH 6.8. When passing from the free form to the adduct with oxalate, the increase is much larger (of about a factor 3), whereas furosemide binding affects only slightly the axial anisotropy and more appreciably the rhombicity of the tensor. The orientations of the tensors are very similar for the free forms as well as for the furosemide adduct (Figure 3, panels A, C, D), with the z-axis, indicating the direction where the magnetic susceptibility is largest, pointing towards histidine 119 and the x-axis, indicating the direction where the magnetic susceptibility is smallest, pointing towards histidine 96. In the adduct with oxalate, the z-axis rotates of about 50°, pointing toward histidine 96 and forming an angle of about 50° with the perpendicular to the plane of the coordinating nitrogen atoms, and the x-axis rotates of about 80°, pointing between histidines 94 and 119, and forming an angle of about 40° with the perpendicular to the plane of the coordinating nitrogen atoms.

PCSs of the high-spin cobalt(II)-substituted hCAII were previously measured for the thiocyanate [46], perchlorate and nitrate adducts [41] and used to predict the magnetic susceptibility anisotropy tensors. In these cases the axis along which the magnitude of the magnetic susceptibility is the largest is very close to the cobalt(II)-N His 119 direction, and the cobalt(II) ion is pentacoordinated with geometry

ranging from trigonal bipyramidal (thiocyanate) to square pyramidal (perchlorate). The trend observed in the magnitude of the magnetic susceptibility anisotropies and the different orientations of the tensors must be related to the presence of differences in the coordination geometry of the metal ion.

Figure 4 shows the splitting of the d orbitals in ideal tetrahedral (T_d), trigonal bipyramidal (D_{3h}), square pyramidal (C_{4v}) and octahedral (O_h) geometries. If in an ideal geometry the ground state is degenerate, the distortions occurring in the protein coordination environment remove the degeneracy, but the excited states are very close in energy. On the other hand, when in ideal geometry the ground state is not degenerate, excited states can be significantly higher in energy.

High spin cobalt(II) has a d^7 external electronic configuration, implying 3 unpaired electrons. When cobalt(II) is four-coordinated, with a pseudo-tetrahedral geometry, the ground state is non degenerate, and the excited states are relatively far in energy (see Figure 4). The zero-field splitting is usually small. In these conditions, the electron relaxation time is relatively slow and $\Delta\chi$ is small (typical values are around 10 ps and 3×10^{-32} m^3, respectively [47]). On the opposite, in idealized octahedral geometry the ground state is triply degenerate: the degeneracy is removed by the non-ideality of the coordination geometry, or by five-coordination in distorted D_{3h} and C_{4v} geometries, in such a way that the excited states are close in energy. In this case, the electron relaxation time becomes faster and $\Delta\chi$ larger (with typical values of 5 ps and 7×10^{-32} m^3, respectively). In fact, the presence of low lying excited states, especially in distorted C_{4v} geometry, makes the anisotropic spin-orbit coupling and the Orbach relaxation mechanism efficient. The faster electron relaxation time determines narrower NMR signals.

In the cobalt(II)-substituted hCAII, in the low-pH form, the cobalt(II) ion, besides the three protein histidines, is also expected to coordinate one or two water molecules: in solution there is an equilibrium of four- and five-coordinated species containing one or two water molecules as ligands [48–51]. In the high-pH form, cobalt(II) is tetracoordinated with OH$^-$ as a fourth ligand that exchanges as H$_2$O via a pentacoordinated intermediate [49]. X-ray structures of the cobalt-substituted crystals obtained

in the presence of ammonium sulfate indicate a tetrahedral geometry at the metal site both at pH 6.0 and 7.8 [52]. The calculated values for the axial anisotropies of the magnetic susceptibility tensor are in agreement with a tetracoordinated cobalt(II) or with an equilibrium of tetracoordinated and pentacoordinated species. The slightly larger anisotropy observed for the higher pH may be due to a conformational variation (e.g., smaller distance of the oxygen atom from the metal, decreased mobility of the oxygen donor) when OH^- is bound with respect to when H_2O is bound [53].

Upon furosemide binding, the magnitude of the tensor anisotropy does not change sizably, thus indicating that the coordination geometry is maintained. Actually, we may expect that in this adduct cobalt(II) is tetracoordinated, as observed in the X-ray structure solved for the zinc hCAII (PDB 1Z9Y).

On the contrary, in the presence of oxalate, the much larger anisotropy indicates that cobalt(II) is fully pentacoordinated [48]: an adduct is thus formed where the ligands are the three protein histidine residues and two oxygen atoms of the oxalate. In distorted pentacoordinated geometries (D_{3h} and C_{4v}, see Fig. 4), in fact, the excited states are closer to the ground state than in tetrahedral geometry because of the vicinity of the energy levels with paired and unpaired electrons. In line with the faster electron relaxation time expected in the presence of a larger anisotropy, a sizable sharpening of the NMR peaks of the adduct between cobalt(II)-hCAII and oxalate is observed.

NMR analysis of the Ni-substituted hCAII and its adduct with furosemide.

The anisotropy of the magnetic susceptibility of the free nickel(II)-substituted hCAII is very small, suggesting that the excited states are far in energy from the ground state. Crystal structures obtained in the presence of ammonium sulfate (PDB 1RZE) indicate that nickel(II) is hexacoordinated, with the nitrogen atoms of the three protein histidines, two water molecules and one sulfate oxygen as ligands [52]. Electronic and CD spectra of the bovine protein suggest the presence of a thermal

equilibrium between two species where the metal ion is coordinated to the three protein histidines and to either two or three water molecules [54].

Again, the low magnetic susceptibility anisotropy of this system can be related to the coordination geometry of the metal. Nickel(II) has a d^8 external electronic configuration, implying 2 unpaired electrons. When nickel(II) is six-coordinated (with pseudo-octahedral geometry) or five-coordinated in square pyramidal geometry, the ground state is singly degenerate and excited states are very far in energy (Figure 4), so that electron relaxation times of 100 ps and very small $\Delta\chi$ are expected, as actually observed. The main mechanism for electron relaxation is in this case the modulation of the zero-field splitting. The orientation of the tensor is not well defined due to the low signal-to-noise ratio and the high rhombicity (the axial and rhombic anisotropies are -0.34×10^{-32} and 0.04×10^{-32} m^3, respectively, using the standard convention $|\Delta\chi_{rh}| \leq 2|\Delta\chi_{ax}|/3$). The axis along which the magnetic susceptibility is largest is pointing towards histidine 94, forming an angle of about 43° with the perpendicular to the plane of the coordinating histidine nitrogen atoms. The axis along which the magnetic susceptibility is smallest is pointing towards histidine 119 (Figure 3E).

The sizable increase in anisotropy observed for nickel(II)-hCAII in the presence of furosemide suggests a change in the coordination geometry of the metal ion upon binding of furosemide. When nickel(II) is four-coordinated in ideal tetrahedral geometry the ground state is triply degenerate. The degeneracy is removed by the non-ideality of the coordination geometry, but still allowing for the excited states to be close in energy. The low-lying excited states arising in pseudo-tetrahedral geometry make Orbach relaxation very efficient, so that the electron relaxation time decreases to values of the order of 1 ps, and $\Delta\chi$ is expected to increase. Intermediate values between those in pseudo-octahedral and in pseudo-tetrahedral geometries are expected for five coordination in trigonal bipyramidal geometry, when the ground state is doubly degenerate. We can thus expect that, in the presence of furosemide, the ligand replaces the water molecules in a tetrahedral arrangement, as observed in the X-ray structure (PDB 1Z9Y)

of the zinc(II) derivative. Therefore, upon complex formation, the coordination number decreases from five/six to four.

The directions of the axes of the tensor are similar to those of the tensors of the cobalt species when free and in its adduct with furosemide, but the three axes are interchanged: the z-axis, indicating the direction where the magnetic susceptibility is largest, points towards histidine 119 in the cobalt form and towards histidine 96 in the nickel-furosemide adduct, and the x-axis, indicating the direction where the magnetic susceptibility is smallest, pointing towards histidine 96 in the cobalt form and towards histidine 94 in the nickel-furosemide adduct. No axis is oriented along the perpendicular to the plane of the three histidine nitrogen atoms.

Conclusions

Paramagnetic NMR has been widely exploited for structure calculation and refinement of metalloproteins, because paramagnetic restraints are highly sensitive to small structural changes. A drawback is the lack of experimental structural information for the so called "blind sphere", i.e. the region around the metal site, which includes the ligands coordinating the paramagnetic metal ion. Furthermore, the chemical shifts of the metal ligands are influenced by both contact and pseudocontact contributions, that are difficult to isolate. On the other hand, the anisotropy of the magnetic susceptibility tensor and its axes directions depend on the electronic structure and on the coordination geometry of the paramagnetic metal ion. Therefore, the evaluation of the $\Delta\chi$ tensors starting from paramagnetic observables (PCSs) measured on nuclei distant from the paramagnetic center can provide information on the coordination geometry of the metal ion. In perspective, the calculation of the $\Delta\chi$ tensor from the molecular structure at the metal site can also be performed from first principles. From a structural model of the metal site, in fact, the molecular g and zero-field splitting tensors can be calculated, and from these quantities, the $\Delta\chi$ tensor [27]. In turn, the comparison of the calculated tensor with the experimental $\Delta\chi$ tensor could allow

14

for a refinement of the coordination geometry of the paramagnetic metal ion: this will be possible by optimizing the molecular structure until a good agreement between calculated and experimental $\Delta\chi$ tensors is achieved (Figure 5).

We have shown that the comparison of the $\Delta\chi$ tensors calculated for the free cobalt(II)-hCAII and for its adducts with the oxalate and furosemide ligands allows for monitoring changes in the coordination of the metal. The similarities in magnitude and orientation of the $\Delta\chi$ tensors when passing from the free form to the adduct with furosemide report on a similar coordination of the metal. On the contrary, the increase in magnitude of the $\Delta\chi$ tensor and the change in its orientation, detected in the presence of oxalate, indicate an increase in the coordination number of the metal. Similarly, in nickel(II)-hCAII, the drastic change in the magnitude of the tensor observed when passing from the free protein to the adduct with furosemide testifies the variation from penta/hexacoordination to tetracoordination. By and large, the high sensitivity of PCSs to the metal coordination sphere can provide a useful tool for a quick screening of ligands on pharmaceutically-relevant targets.

Acknowledgments

References

1. Bertini I, McGreevy KS, Parigi G (2012) NMR in systems biology. Wiley

2. Clore M, Potts J (2012) Recent developments in biomolecular NMR. RSC Publ, Cambridge

3. Hiruma Y, Hass MAS, Kikui Y, et al (2013) The structure of the cytochrome p450cam-putidaredoxin complex determined by paramagnetic NMR spectroscopy and crystallography. J Mol Biol 425:4353–4365. doi: 10.1016/j.jmb.2013.07.006

4. Andrałojć W, Hiruma Y, Liu W-M, et al (2017) Identification of productive and futile encounters in an electron transfer protein complex. Proc Natl Acad Sci U S A. doi: 10.1073/pnas.1616813114

5. Cerofolini L, Fields GB, Fragai M, et al (2013) Examination of Matrix Metalloproteinase-1 in Solution: A PREFERENCE FOR THE PRE-COLLAGENOLYSIS STATE. J Biol Chem 288:30659–30671. doi: 10.1074/jbc.M113.477240

6. Tang C, Iwahara J, Clore GM (2006) Visualization of transient encounter complexes in protein-protein association. Nature 444:383–386. doi: 10.1038/nature05201

7. Rumpel S, Becker S, Zweckstetter M (2008) High-resolution structure determination of the CylR2 homodimer using paramagnetic relaxation enhancement and structure-based prediction of molecular alignment. J Biomol NMR 40:1–13. doi: 10.1007/s10858-007-9204-4

8. Saio T, Yokochi M, Kumeta H, Inagaki F (2010) PCS-based structure determination of protein–protein complexes. J Biomol NMR 46:271–280. doi: 10.1007/s10858-010-9401-4

9. Brewer KD, Bacaj T, Cavalli A, et al (2015) Dynamic binding mode of a Synaptotagmin-1–SNARE complex in solution. Nat Struct Mol Biol 22:555–564. doi: 10.1038/nsmb.3035

10. Kim YC, Tang C, Clore GM, Hummer G (2008) Replica exchange simulations of transient encounter complexes in protein-protein association. Proc Natl Acad Sci 105:12855–12860. doi: 10.1073/pnas.0802460105

11. Gochin M, Roder H (1995) Use of pseudocontact shifts as a structural constraint for macromolecules in solution. Bull Magn Reson 17:1–4.

12. Banci L, Bertini I, Bren KL, et al (1996) The use of pseudocontact shifts to refine solution structures of paramagnetic metalloproteins: Met80Ala cyano-cytochrome c as an example. JBiolInorgChem 1:117–126.

13. Bertini I, Donaire A, Jim?nez B, et al (2001) Paramagnetism-based Versus Classical Constraints: An Analysis of the Solution Structure of Ca Ln Calbindin D9k. JBiomolNMR 21:85–98.

14. Bertini I, Kursula P, Luchinat C, et al (2009) Accurate solution structures of proteins from X-ray data and minimal set of NMR data: calmodulin peptide complexes as examples. J Am Chem Soc 131:5134–5144.

15. Banci L, Bertini I, Cavallaro G, et al (2004) Paramagnetism-based restraints for Xplor-NIH. JBiomolNMR 28:249–261.

16. Balayssac S, Bertini I, Luchinat C, et al (2006) 13C direct detected NMR increases the detectability of residual dipolar couplings. J Am Chem Soc 128:15042–15043.

17. Sala D, Giachetti A, Luchinat C, Rosato A (2016) A protocol for the refinement of NMR structures using simultaneously pseudocontact shift restraints from multiple lanthanide ions. J Biomol NMR 66:175–185. doi: 10.1007/s10858-016-0065-6

18. Schmitz C, Bonvin AMJJ (2011) Protein-protein HADDocking using exclusively pseudocontact shifts. J Biomol Nmr 50:263–266. doi: 10.1007/s10858-011-9514-4

19. Rinaldelli M, Ravera E, Calderone V, et al (2014) Simultaneous use of solution NMR and X-ray data in REFMAC5 for joint refinement/detection of structural differences. Acta Crystallogr D Biol Crystallogr 70:958–967. doi: 10.1107/S1399004713034160

20. Chou JJ, Li S, Klee CB, Bax A (2001) Solution structure of Ca2+ calmodulin reveals flexible hand-like properties of its domains. Nat Struct Mol Biol 8:990–997.

21. Bertini I, Calderone V, Cerofolini L, et al (2012) The catalytic domain of MMP-1 studied through tagged lanthanides. FEBS Lett 586:557–567.

22. Rinaldelli M, Carlon A, Ravera E, et al (2015) FANTEN: a new web-based interface for the analysis of magnetic anisotropy-induced NMR data. J Biomol NMR 61:21–34. doi: 10.1007/s10858-014-9877-4

23. Schmitz C, Stanton-Cook MJ, Su X-C, et al (2008) Numbat: an interactive software tool for fitting Δχ-tensors to molecular coordinates using pseudocontact shifts. J Biomol NMR 41:179–189. doi: 10.1007/s10858-008-9249-z

24. Bertini I, Luchinat C, Parigi G, Ravera E (2017) NMR of paramagnetic molecules: applications to metallobiomolecules and models.

25. Pennanen TO, Vaara J (2008) Nuclear magnetic resonance chemical shift in an arbitrary electronic spin state. Phys Rev Lett 100:133002. doi: 10.1103/PhysRevLett.100.133002

26. Van den Heuvel W, Soncini A (2012) NMR chemical shift in an electronic state with arbitrary degeneracy. Phys Rev Lett 109:073001. doi: 10.1103/PhysRevLett.109.073001

27. Benda L, Mareš J, Ravera E, et al (2016) Pseudo-Contact NMR Shifts over the Paramagnetic Metalloprotein CoMMP-12 from First Principles. Angew Chem Int Ed Engl 55:14713–14717. doi: 10.1002/anie.201608829

28. Ravera E, Parigi G, Luchinat C (2017) Perspectives on paramagnetic NMR from a life sciences infrastructure. J Magn Reson 282:154–169. doi: 10.1016/j.jmr.2017.07.013

29. Supuran CT (2013) Carbonic anhydrases: from biomedical applications of the inhibitors and activators to biotechnological use for CO2 capture. J Enzyme Inhib Med Chem 28:229–230. doi: 10.3109/14756366.2013.761876

30. Bertini I, Luchinat C, Scozzafava A (1978) Binding affinity of bicarboxylate ions for cobalt(II) bovine carbonic anhydrase. BioinorgChem 9:93–100.

31. Bertini I, Luchinat C, Scozzafava A (1978) A 31P NMR study of phosphate in presence of cobalt(II)- and copper(II)- substituted bovine carbonic anhydrase B. FEBS Lett 93:251–254.

32. Nettles WL, Song H, Farquhar ER, et al (2015) Characterization of the Copper(II) Binding Sites in Human Carbonic Anhydrase II. Inorg Chem 54:5671–5680. doi: 10.1021/acs.inorgchem.5b00057

33. Bertini I, Luchinat C, Monnanni R, Scozzafava A (1982) Different behavior of sulfonamides with respect to copper- substituted bovine and human carbonic anhydrases. JInorgBiochem 16:155–160.

34. Bertini I, Canti G, Luchinat C, Borghi E (1983) Investigation of the system copper(II) carbonic anhydrase and HCO3-/CO2. JInorgBiochem 18:221–229.

35. Bertini I, Luchinat C, Scozzafava A (1978) Evidence of exchangeable protons in the acidic form of manganese(II) bovine carbonic anhydrase B. FEBS Lett 87:92–94.

36. Moratal JM, Jiménez HR, Castells J, et al (1992) 1H NMR and UV-vis spectroscopic characterization of sulfonamide complexes of nickek(II)-carbonic anhydrase. Resonance assignments based on NOE effects. J Inorg Biochem 45:231–243. doi: 10.1016/0162-0134(92)84012-C

37. Bertini I, Borghi E, Luchinat C (1978) Characterization of nickel(II) bovine carbonic anhydrase and its inhibitor derivatives. BioinorgChem 9:495–504.

38. Moratal JM, Martínez-Ferrer M-J, Donaire A, et al (1991) Spectroscopic studies of nickel(II) carbonic anhydrase and its adducts with inorganic anions. J Chem Soc Dalton Trans 3393–3399. doi: 10.1039/DT9910003393

39. Cerofolini L, Giuntini S, Louka A, et al (2017) High-Resolution Solid-State NMR Characterization of Ligand Binding to a Protein Immobilized in a Silica Matrix. J Phys Chem B 121:8094–8101. doi: 10.1021/acs.jpcb.7b05679

40. Bertini I, Luchinat C, Pierattelli R, Vila AJ (1992) The interaction of acetate and formate with cobalt carbonic anhydrase. An NMR study. Eur J Biochem 208:607–615.

41. Banci L, Dugad LB, La Mar GN, et al (1992) 1H Nuclear Magnetic Resonance investigation of cobalt(II) substituted carbonic anhydrase. BiophysJ 63:530–543.

42. Hunt JB, Rhee MJ, Storm CB (1977) A rapid and convenient preparation of Apocarbonic Anhydrase. AnalBiochem 55:614–617.

43. Bertini I, Luchinat C, Parigi G (2002) Paramagnetic constraints: an aid for quick solution structure determination of paramagnetic metalloproteins. Concepts Magn Reson 14:259–286.

44. Avvaru BS, Kim CU, Sippel KH, et al (2010) A Short, Strong Hydrogen Bond in the Active Site of Human Carbonic Anhydrase II. Biochemistry (Mosc) 49:249–251. doi: 10.1021/bi902007b

45. Bertini I, Janik MBL, Lee Y-M, et al (2001) Magnetic Susceptibility Tensor Anisotropies for a Lanthanide Ion Series in a Fixed Protein Matrix. J Am Chem Soc 123:4181–4188.

46. Bertini I, Jonsson B-H, Luchinat C, et al (1994) Strategies of signal assignments in paramagnetic metalloproteins. An NMR investigation of the thiocyanate adduct of the cobalt(II)-substituted human carbonic anhydrase II. J Magn Reson B 104:230–239.

47. Bertini I, Luchinat C, Parigi G, Pierattelli R (2005) NMR of paramagnetic metalloproteins. ChemBioChem 6:1536–1549.

48. Bertini I, Luchinat C (1983) Cobalt(II) as a probe of the structure and function of carbonic anhydrase. AccChemRes 16:272–279.

49. Koenig SH, Brown III RD, Bertini I, Luchinat C (1983) Water exchange at the active site of carbonic anhydrase. A synthesis of the OH- and H2O-models. BiophysJ 41:179–187.

50. Bertini I, Lanini G, Luchinat C (1983) Equilibrium species in cobalt(II) carbonic anhydrase. J Am Chem Soc 105:5116–5118.

51. Avvaru BS, Arenas DJ, Tu C, et al (2010) Comparison of solution and crystal properties of Co(II)–substituted human carbonic anhydrase II. Arch Biochem Biophys 502:53–59. doi: 10.1016/j.abb.2010.07.010

52. Hakansson K, Wehnert A, Liljas A (1994) X-ray analysis of metal substituted human carbonic anhydrase II derivatives. Acta Crystallogr D50:93–100.

53. Bertini I, Canti G, Luchinat C, Mani F (1981) pH-dependent properties of a CoN4(OH2) chromophore: a spectroscopic model of cobalt carbonic anhydrase. Inorg Chem 20:1670–1673.

54. Bertini I, Borghi E, Luchinat C, Monnanni R (1982) Nickel carbonic anhydrase: a re-examination of the electronic spectra with the help of CD spectra. Inorganica Chim Acta 67:99–102.

Captions to the Figures.

Figure 1. Cartoon representation of the X-ray structure of zinc(II)-hCAII (PDB 3KS3) with indicated the active site ligands (A) and structural formula of the oxalate (B) and furosemide (C) ligands.

Figure 2. Correlation plots between experimental and calculated PCS collected for the cobalt(II)- and nickel(II)-substituted carbonic anhydrase. *The Q value for the free nickel(II) form is calculated taking into account a tolerance of 0.02 ppm, which is the estimated error of PCSs.

Figure 3. Stereo cross-eyed graphical representation of the magnetic susceptibility anisotropy tensor orientations and the PCS isosurfaces of 1 (blue) and -1 (red) ppm obtained for: uninhibited cobalt(II)-hCAII at pH 5.8 (A), cobalt(II)-hCAII bound to oxalate (B), uninhibited cobalt(II)-hCAII at pH 6.8 (C), cobalt(II)-hCAII bound to furosemide (D), uninhibited nickel(II)-hCAII (E) and nickel(II)- hCAII bound to furosemide (F). The x, y and z axes (corresponding to the directions with the smallest, intermediate and largest magnetic susceptibility) are represented as red, yellow and blue arrows, respectively; the positive isosurfaces are in blue and the negative are in red.

Figure 4. Population of the electronic d orbitals in idealized tetrahedral and octahedral geometry for high spin cobalt(II) and nickel(II).
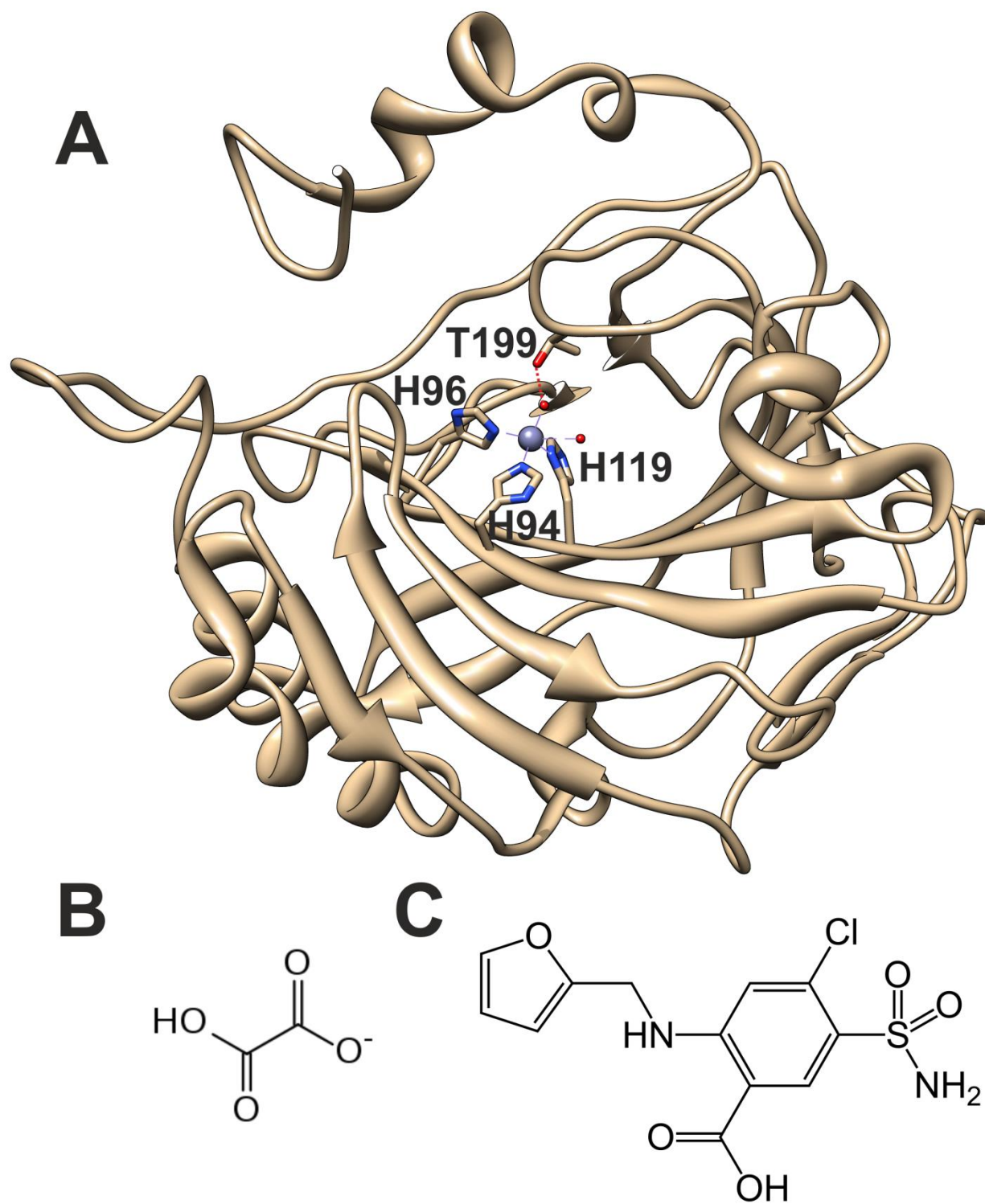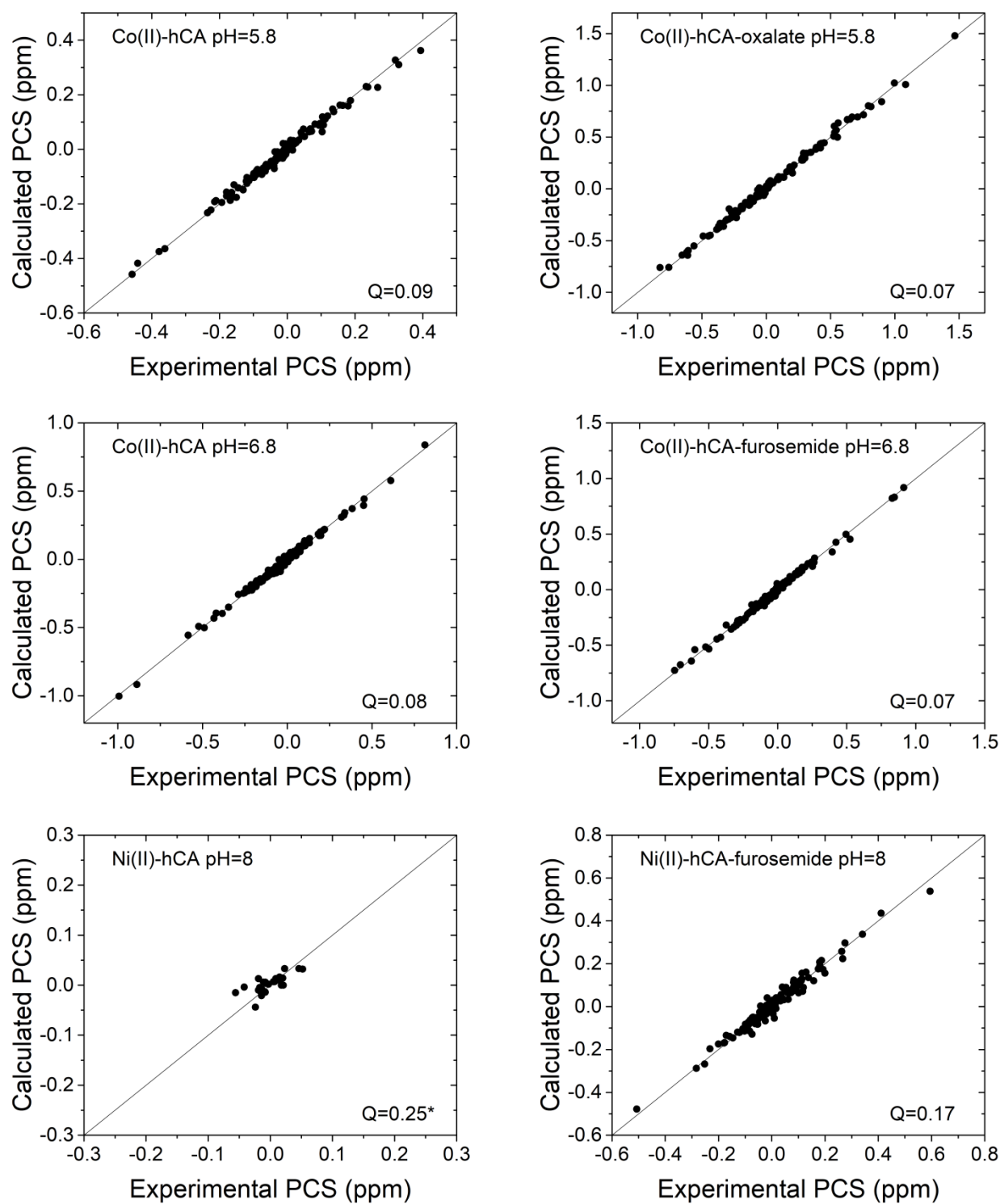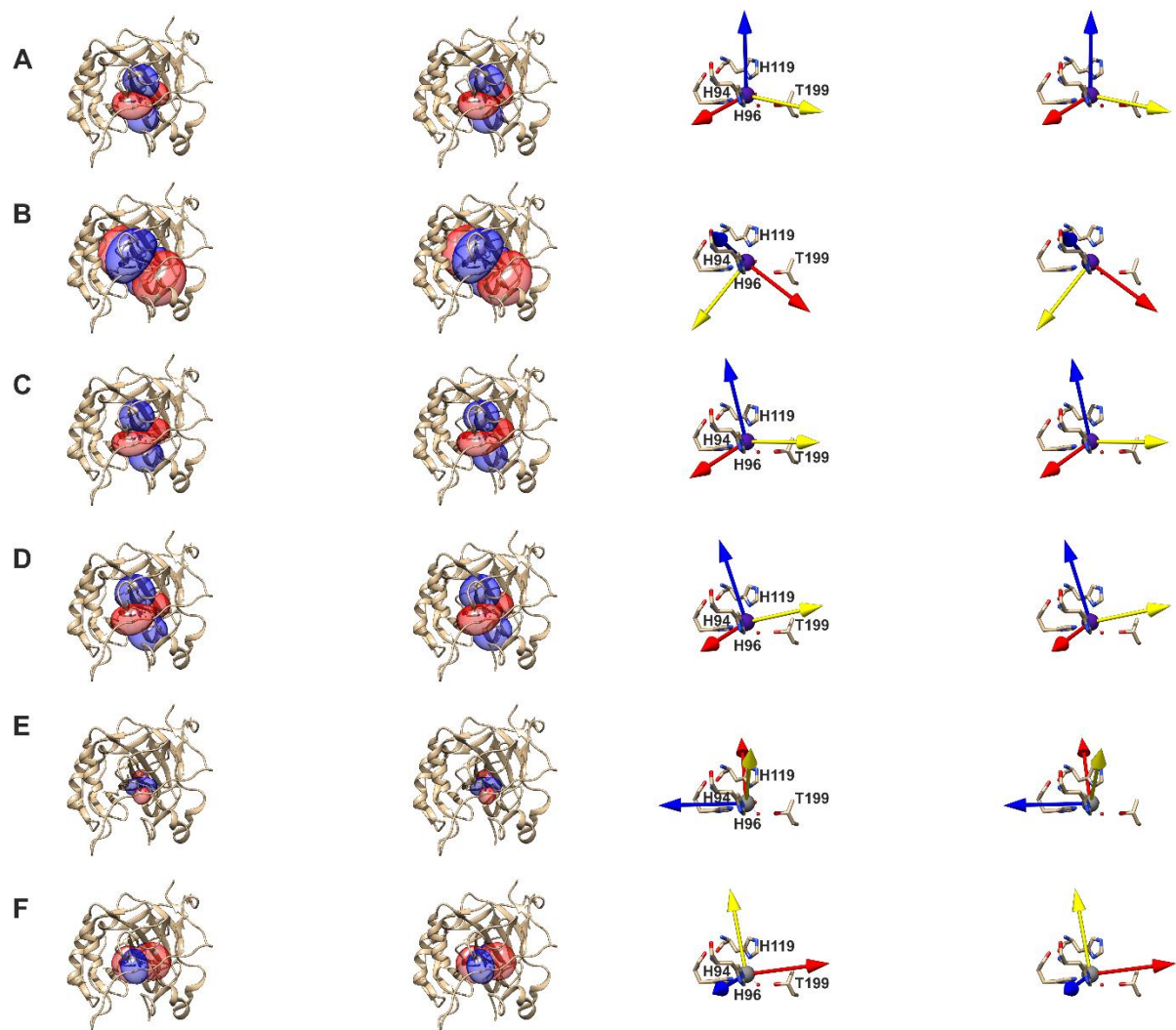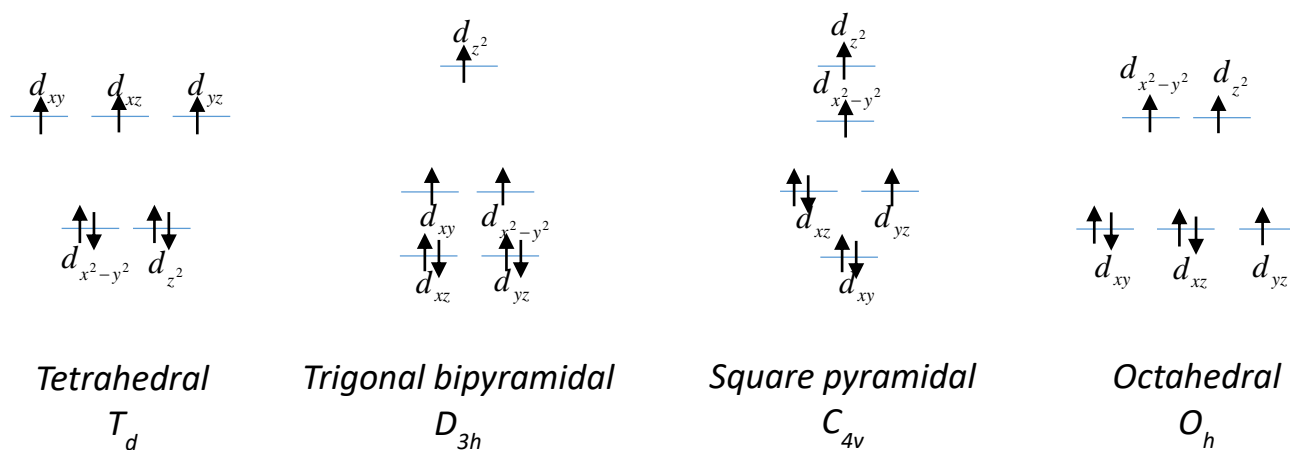
Figure 1.

Figure 2.

Figure 3.

Cobalt(II)

Tetrahedral T_d	*Trigonal bipyramidal* D_{3h}	*Square pyramidal* C_{4v}	*Octahedral* O_h

Nickel(II)

Octahedral O_h	*Square pyramidal* C_{4v}	*Trigonal bipyramidal* D_{3h}	*Tetrahedral* T_d

Figure 4.